ACS APPLIED OPTICAL MATERIALS

pubs.acs.org/acsaom Letter

Exceptional Electrochromic Solar Modulation Using Polyanionic Dopant Templated Poly(diphenylamine) Thin Films

Simranjit Grewal, Terefe G. Habteyes,* Wassie M. Takele, Dongchang Chen, John K. Grey,* and Nathan T. Hahn*

Cite This: ACS Appl. Opt. Mater. 2024, 2, 361−367 Read Online

ACCESS | Metrics & More | Article Recommendations | Supporting Information

ABSTRACT: We report poly(diphenylamine) thin films with exceptional optical clarity (T_{vis} ≥ 0.80) and electrochromic solar modulating ability (ΔT_{sol} ≥ 0.60). Electropolymerizing diphenylamine in the presence of a polyanionic acid dopant is critical to achieving high macroscale uniformity and smoothness, which minimizes optical scattering and maximizes electrochromic response throughout the visible (>400 nm) and near-infrared (>700 nm) spectral ranges. We then use combinations of near- and far-field spectroscopies and their imaging modes to elucidate the roles of dopants in directing polymerization and resulting chain conformational order. By comparing small molecule and polymeric sulfonic acid dopants, we determine that the latter template poly(diphenylamine) polymerization to achieve superior morphological characteristics responsible for high electrochromic contrast. The results demonstrate the potential of these polymeric materials as active layers or components in smart window applications.

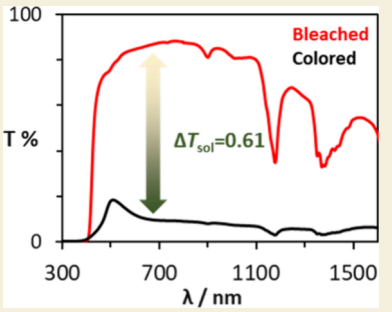

KEYWORDS: *electrochromic materials, smart windows, polydiphenylamine, ΔT_{sol}, morphology, templated polymerization, polystyrenesulfonic acid*

Electrochromic windows have been recognized as a potentially valuable means of reducing building energy use associated with space heating/cooling by enabling on-demand control of redox-dependent solar energy transmission as so-called "smart windows".[1,2] The primary metric in controlling solar energy admission through the window is the solar transmittance contrast, ΔT_{sol}, which is the difference between the normalized solar transmittance values of the window in its blocking or "colored" (low T_{sol}) and transparent or "bleached" (high T_{sol}) states. Values of ΔT_{sol} (a primary component of window solar heat gain modulation, ΔS_{HGC}) of at least 0.5−0.6 are deemed critical for practical smart window technologies[1,3] and require substantial modulation of both visible and near-infrared (NIR) transmittance in the electrochromic material(s). Current state-of-the-art electrochromic smart windows typically utilize WO_3 thin films and exhibit overall ΔT_{sol} values less than 0.4, although this device-level value also includes transmittance losses through the entire device stack.[2] Such metal-oxide film devices also tend to be expensive due to the use of vacuum-based deposition processes, further limiting their extent of deployment and impact on energy and climate concerns. It is therefore of great interest for smart window applications to reduce the cost of the electrochromic materials while increasing the ΔT_{sol} for continued advancement and widespread implementation.

Organic electrochromic films deposited using ambient temperature, solution-based processes could potentially reduce both materials and processing costs while relying less on strategically critical minerals compared to existing technology.[4−7] However, conjugated polymers previously used for electrochromic applications, such as polydialkoxythiophenes, polypyrroles, or polyaniline (PANI), exhibit nonideal spectral characteristics (i.e., inverted visible and NIR responses), often preventing high ΔT_{sol} values from being attained.[4,5] In fact, ΔT_{sol} values are almost never reported for polymer electrochromic materials or devices with rare exceptions being several studies describing devices in which PANI is integrated with one or more complementary inorganic electrochromic materials (see Table S1, Supporting Information).

Poly(diphenylamine) (PDPA), a p-type conjugated polyarylamine with chemical structures similar to PANI, has a more ideal redox potential window and improved vis−NIR modulation ability,[8−10] which makes it a strong candidate for achieving high ΔT_{sol} values if films can be deposited with high optical clarity. Previous anodic electropolymerization studies of PDPA typically involved halide or small molecule dopants[10−12] that produce nonideal thin films in terms of thickness or optical quality although ΔT_{sol} values were not reported.[7,9] Factors, such as insufficient polymerization during early stages

Received: November 20, 2023
Revised: February 13, 2024
Accepted: February 14, 2024
Published: February 19, 2024

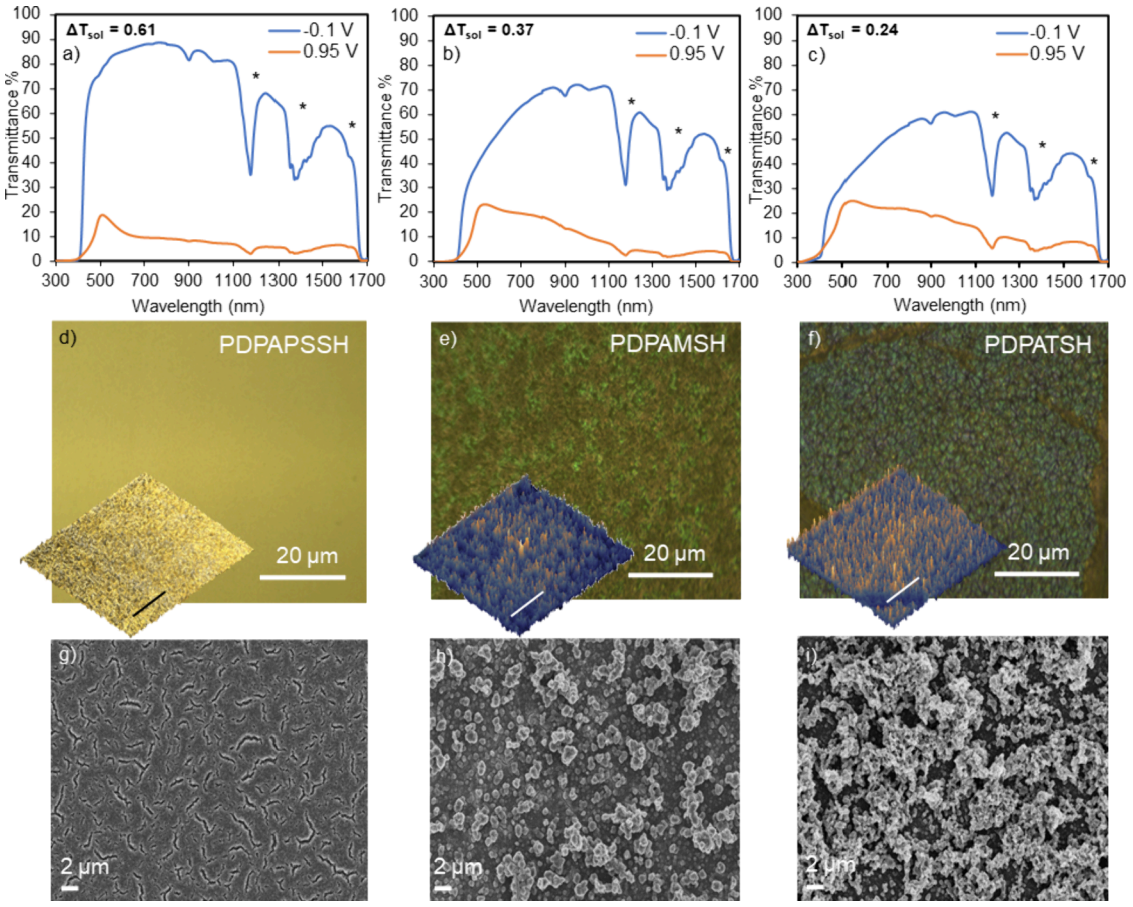

Figure 1. (a–c) Spectro-electrochemical responses from each PDPA-dopant variant on ITO-glass: (a) PSSH, (b) MSH, and (c) TSH held at the indicated potentials vs Ag/AgCl. Absorption features corresponding to the electrolyte are indicated by "*". Integrated ΔT_{sol} values are given for each of these examples. (d–f) Optical images of each PDPA type: (d) PSSH, (e) MSH, and (f) TSH (field of view = 70 μm). Profiles are shown for each image to provide a qualitative reference for surface roughness. (g–i) SEM images for each PDPA variant: (g) PSSH, (h) MSH, and (i) TSH.

of film growth, can lead to partial film dissolution and delamination as well as hazing due to larger morphological features and increased light scattering.

In the following, we show that electropolymerization using a polymeric dopant, namely, poly(4-styrenesulfonic acid) (PSSH), produces PDPA thin films of high optical quality, as observed earlier with PANI.[13,14] Examination of electrochromic properties on the laboratory scale with model devices (see Scheme S1 in the Supporting Information for device geometries studied) reveals exceptionally large ΔT_{sol} values ($\geq$0.6) which, to our knowledge, are the largest recorded for an all-polymer thin film. We then use new combinations of far- and near-field spectroscopic and microscopic probes to elucidate critical structure–property information underpinning high electrochromic contrast by comparing PDPA thin films polymerized with PSSH and related small molecule sulfonic acid dopants. The results indicate that PSSH templates PDPA polymerization favoring high intra- and interchain order and, likewise, better thin film morphological characteristics. We posit that refinements of electropolymerization and redox cycling conditions (viz., electrolyte and solvents) could further improve ΔT_{sol} and long-term stability in full scale devices.

Figure 1 shows electrochromic switching contrast as changes in percent transmittance for each PDPA sample measured in an electrolyte containing 0.2 M $LiClO_4$ dissolved in propylene carbonate (PC). Cycling potentials between −0.1 and 0.95 V access reduced and oxidized PDPA forms, and the ΔT_{sol} values are calculated by integrating the transmittance spectra multiplied by the normalized AM1.5G solar spectrum (see Figure S6, Supporting Information for details). Comparing each variant, the PSSH doped sample (Figure 1a) shows the largest electrochromic contrast with a ΔT_{sol} of 0.61 enabled by exceptional utilization of visible–NIR light, whereas the methanesulfonic acid (MSH) and *p*-toluenesulfonic acid (TSH) doped samples (Figure 1b,c) exhibit considerably lower values of 0.37 and 0.24, respectively. Simple inspection of transmittance spectra line shapes reveals improved spectral coverage and significantly lower scattering contributions from the PSSH doped sample. Scattering is most apparent within the visible range, leading to significant differences in integrated visible (luminous) transmittance (T_{vis} or T_{lum}), with a maximal value of 0.8 reached for PSSH doping (see Figure S5, Supporting Information). Generally, the films transition between slightly green (colored) and slightly yellow (bleached) color states (see Figures S1 and S2 and Scheme S1, Supporting Information). The superior electrochromic performance of PDPA:PSSH thin films originates from high optical quality indicating favorable polymer–dopant interactions and high chain ordering necessary for achieving high electrochromic contrast.[14] The measured broadband ΔT_{sol} value for PDPA:PSSH in Figure 1 is the highest reported to date for a polymeric electrochromic film. Interestingly, such values are commonly absent from the electrochromic polymer literature, and instead, ΔT values are given only at the

https://doi.org/10.1021/acsaom.3c00421
ACS Appl. Opt. Mater. 2024, 2, 361–367

wavelength of maximum contrast. The effective broadband electrochromic contrast afforded by PDPA is thus particularly valuable in this context and suggests that full devices (incorporating a complementary cathodically coloring counter electrode) could yield even greater spectral modulating performance. Additional optical and electrochemical characterizations, such as electrochromic cycling, are shown in the Supporting Information (i.e., Figures S1 and S7).

We now turn our attention to understanding the molecular factors responsible for achieving a high quality morphology and, consequently, high ΔT_{sol} values. Morphological insights of sulfonic acid dopant effects are obtained using optical and scanning electron microscopy (SEM) imaging shown in Figure 1d–f,g–i, respectively. In both imaging modes, PSSH doped thin films show much finer textural features than the MSH or TSH forms. SEM images reveal features resembling fissures with characteristic size scales of up to 1 μm, probably from rapid film drying following electropolymerization and rinsing. However, surface cracks do not appear to adversely affect optical qualities and additional cross-sectional imaging shows that film thickness (ca. 500–600 nm) was uniform across the entire sample (see Figures S8–10, Supporting Information). Larger grain features in the MSH and TSH doped thin films resemble those frequently observed in related electropolymerized polyarylamine thin films[15,16] that lead to increased scattering and nonuniform surface coverage which are unfavorable for electrochromic applications.[17] These marked differences in morphologies with the dopant type and their electrochromic performance (ΔT_{sol}) suggest large deviations in both the polymerization mechanism and resultant polymer–dopant interactions. The finer textures of PDPA:PSSH thin films are suggestive of intimate mixing or perhaps copolymerization with diphenylamine monomers, which are possible outcomes of the proposed templated polymerization mechanism. While intriguing, this is rarely observed in electropolymerization of polyarylamines, although recent work involving templated deposition of PANI by a Langmuir–Blodgett technique produced thin films of high crystallinity.[18]

Vibrational spectra of as-deposited PDPA samples with the various sulfonic acid dopants were measured using FT-IR absorption and Raman scattering spectroscopies that can expose further details about the molecular structure and local chain order. Figure 2a shows FT-IR absorption spectra of each form, and film thicknesses were comparable for all samples. Distinct transitions corresponding to PDPA and dopant molecules are resolved, and each sample type displays characteristic vibrations from CC stretching and bending modes appearing at ca. 1500–1600 and 600–1000 cm^{-1}, respectively, along with CH bending character at ca. 1300–1400 cm^{-1}.[19] Motions involving sulfoxo groups are apparent at ca. 1100–1400 cm^{-1} and absorption patterns reflect the nature of each dopant (i.e., aromatic vs aliphatic sulfonic acids).[20] C═N stretching character is also evident at ~1550 cm^{-1} as expected from imine functionalities linking backbone diphenyl groups.[21] FT-IR spectra indicate that PDPA structures are similar but do not completely capture chain ordering and morphological details that profoundly influence the electrochromic properties. For the case of PSSH, X-ray photoelectron spectra (XPS) reveal that the dopant is fully integrated into the film structure and the as-deposited film contains a relatively balanced mixture of deprotonated (anionic) PSS^- groups and protonated (neutral) PSSH groups (see Figure S11, Supporting Information). Furthermore, PSSH levels are enriched at the surface of the PDPA film following electrochemical treatments in a 0.2 M $LiClO_4$/PC electrolyte, which might also promote stability due to insolubility of this dopant in PC. Unfortunately, film roughness of the MSH and TSH doped samples were too large to obtain reliable XPS data for comparison.

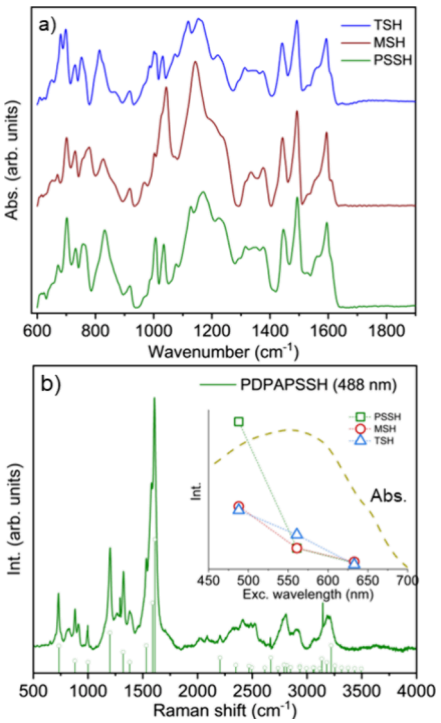

Figure 2. (a) IR absorption spectra of PDPA with various sulfonic acid dopants. (b) Resonance Raman spectra of PDPA:PSSH (488 nm excitation) and simulated intensities. Inset: Comparison of integrated Raman intensities as a function of excitation wavelength for all PDPA variants with electronic absorption spectra of PDPA.

Raman spectra offer additional perspectives and further benefit from strong resonance enhancement effects often observed in related polyarylamine materials.[19] Raman spectra were measured using several laser excitation sources spanning the PDPA electronic absorption spectral range (i.e., 325–1064 nm) with comparable power densities (~1 kW/cm^2). Figure 2b displays a representative resonance Raman line shape for PDPA:PSSH excited with 488 nm light, which exhibits pronounced overtone and combination band features originating from the reduced form of PDPA. While these features were present for all thin film samples, resonance enhancement effects were strongest in the PDPA:PSSH variant (Figure 2b indicating higher intrachain order. Raman intensity simulations (including overtones and combination bands) were undertaken to qualitatively assess this effect (see eqs S1–S3 and related text in Supporting Information) with an example fit included in Figure 2b are shown as stick spectrum. By adjusting the phenomenological excited state lifetime (i.e., damping factor), we show—in an ad-hoc manner—that substantially larger intensities in the PDPA:PSSH sample correspond to longer-lived dynamics consistent with lower disorder-induced amplitude losses.

We next sought to connect the molecular level structure to morphology-dependent electrochromic performance by performing scattering type near-field scanning optical microscopy (s-SNOM) on PDPA thin films. s-SNOM uses broadly tunable MIR excitation to generate morphology-dependent chemical

https://doi.org/10.1021/acsaom.3c00421
ACS Appl. Opt. Mater. 2024, 2, 361–367

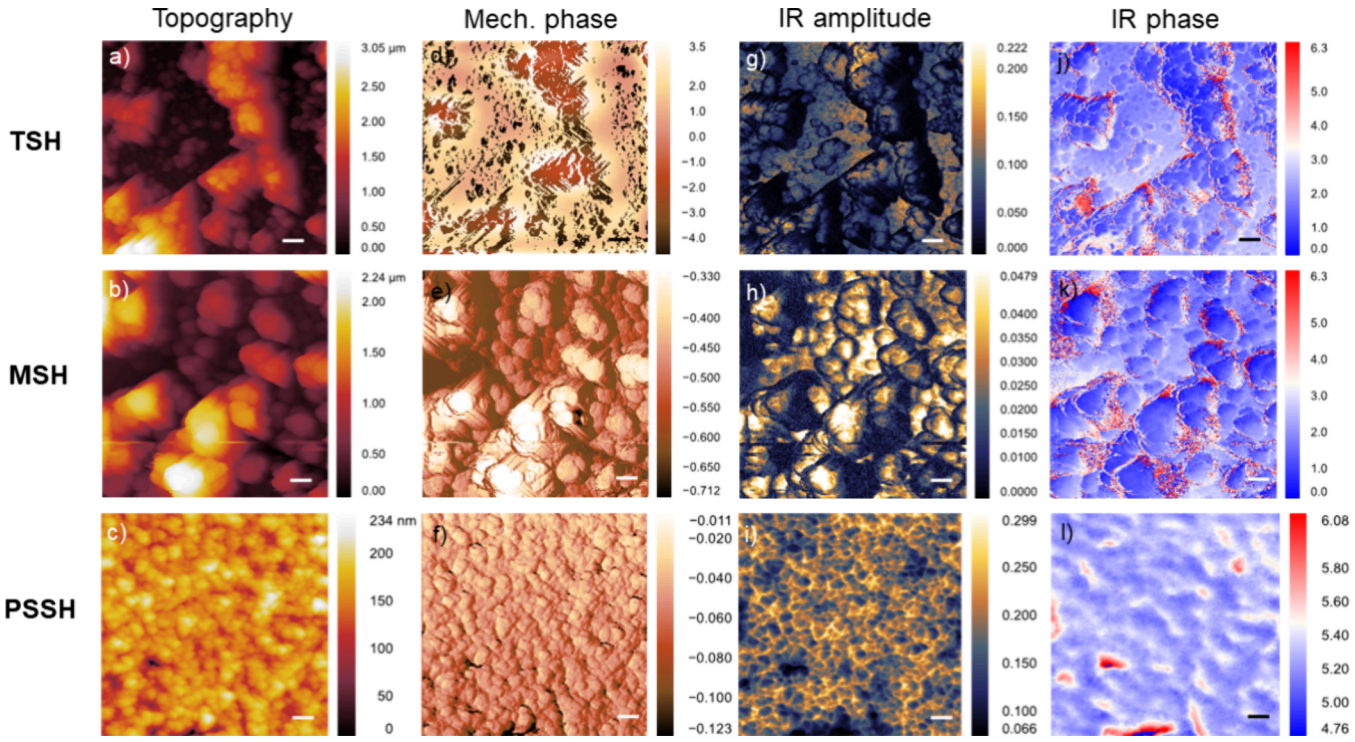

Figure 3. s-SNOM images of PDPA thin films using an excitation frequency of 1550 cm^{-1} with the various sulfonic acid dopants (TSH, MSH, and PSSH) showing topography (a–c), mechanical phase shift (d–f), IR amplitude (S_4, g–i), and IR phase (Ω_4, j–l). Image field of view for all samples was 10 × 10 μm (scale bar = 1 μm).

Scheme 1. Illustration of Proposed Dopant Interactions with PDPA

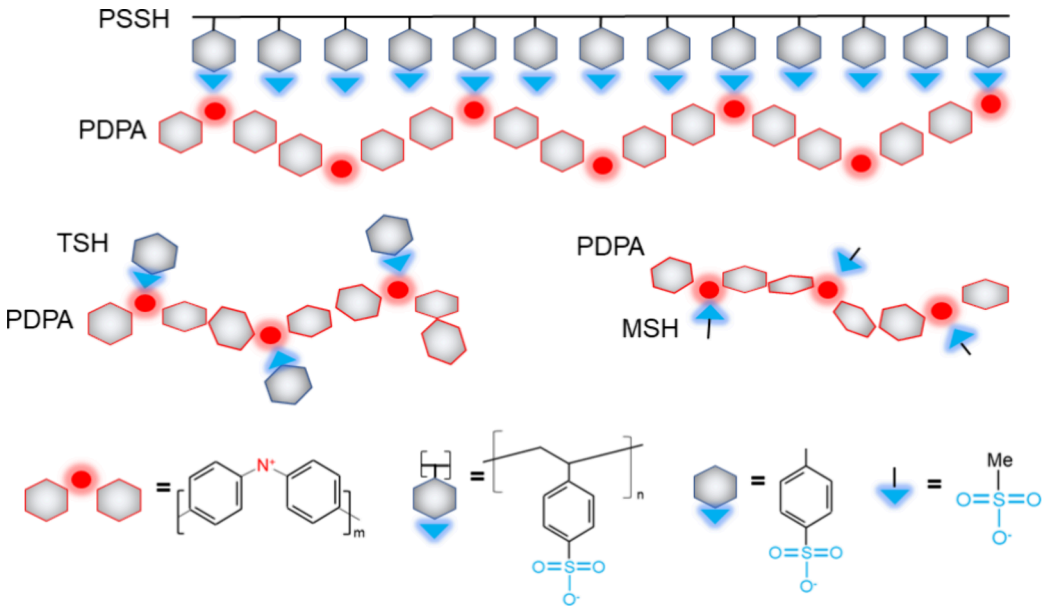

maps of each dopant variant which are shown in Figure 3 (experimental details and additional images are provided in the Supporting Information, Figures S19–22). s-SNOM images excited at multiple PDPA vibrational frequencies (see Figure 2a) showed little change in appearance, although the magnitudes of the amplitude and phase (i.e., real and imaginary parts of the complex dielectric function) were excitation-dependent. Comparing topographies and mechanical phase contrast reveals stark differences in morphology, consistent with SEM images in Figure 1. MSH and TSH dopants exhibit large topographical features resembling spheroids up to several micrometers, whereas features in PSSH doped PDPA thin films have much smaller characteristic size scales (~100 nm). Tip–sample interactions reflected in the mechanical phase contrast showed larger deviations in MSH and TSH doped samples due to greater surface hardness probably from higher surface charge densities. Conversely, PSSH doped films displayed much "softer" tip–sample interactions consistent with less surface charge consistent with XPS results (see Supporting Information).

https://doi.org/10.1021/acsaom.3c00421
ACS Appl. Opt. Mater. 2024, 2, 361–367

IR amplitude images show strong contrast that further highlights morphological differences between each dopant form. Namely, large domain features in MSH and TSH films show greater IR reflectivity (i.e., $\mathrm{Re}[\varepsilon_r(\omega)]$), consistent with greater metallic character[22] which varies significantly over the scan field of view. Corresponding images from PSSH doped films reveal much more uniform IR amplitude due to a finer texture and probably less localized surface charge. Comparing these trends with the IR phase contrast (i.e., $\mathrm{Im}[\varepsilon_r(\omega)]$) helps better resolve morphology-dependent surface features since this contribution reports the extent of excitation absorption. Larger IR phase contrast correlates with lower reflectivity, revealing abrupt zone boundaries in both MSH and TSH doped thin films that may contribute to poor charge transport and electrochromic contrast. PSSH-doped PDPA thin film morphologies again display more uniform features indicating better phase continuity and connectivity seen in other ordered conjugated polymers.[23] While some regions of high IR phase contrast are apparent, the absence of abrupt boundaries surrounding domains suggests better charge transport characteristics and lower trapping and recombination efficacies in addition to improved optical qualities.

In summary, we have demonstrated exceptional ΔT_{sol} values for an anodically colored polymeric electrochromic thin film produced through a solution-based technique under ambient conditions. This finding highlights the potential value of PDPA as a broadband (vis−NIR) active electrochrome for dynamic solar control with the potential for large-scale, sustainable implementation. The incorporation of the PSSH polyanionic dopant has dual roles in both templating electropolymerization, which produces PDPA chains of much higher conformational order, and ensuring charge neutrality. Although chain connectivity is similar between dopants as evidenced from IR absorption spectra, larger intensity enhancements from resonance Raman spectra reveal PSSH doped samples are consistent with improved ordering qualities. This concept is illustrated in Scheme 1 where attractive Coulombic interactions occur along with regular spacing intervals between charged substituents. Higher local ordering likewise promotes lower heterogeneity and, consequently, superior nano- to microscopic morphology characteristics essential for high electrochromic contrast as revealed by s-SNOM studies. Large phase separated domains with abrupt boundaries in the MSH and TSH doped thin films cause increased scattering and probably promote unwanted charge trapping and recombination as revealed from s-SNOM IR amplitude and phase imaging. On the other hand, PSSH doped PDPA films displayed much higher uniformity consistent with improved charge transport necessary for high electrochromic contrast. Further advancements in understanding and promoting the long-term stability of these films under relevant conditions, particularly in full devices will be vital for assessing their ultimate potential for smart window applications. Stabilities of polymer materials under solar irradiance (especially UV) can be limited, although degradation mitigation strategies do exist.[24,25] Furthermore, the chemically similar polyarylamine PANI has shown stable electrochromic performance during harsh space-like environmental testing.[26] Combining this level of environmental stability with the high ΔT_{sol} of PDPA:PSSH could enable low-cost, high-performance electrochromic smart window technologies with great potential for building energy savings if integrated with an appropriate complementary cathodic coloring counter electrode.

EXPERIMENTAL METHODS

Electropolymerization of PDPA

All chemical reagents were purchased from Sigma-Aldrich except where indicated. DPA was dissolved in ethanol (99.5%) at a 0.01 M concentration along with 0.3 M sulfonic acid dopant: PSSH (MW ∼ 75,000, 18 wt % in water), MSH (70 wt % in water), and TSH (monohydrate, 98.5%). ITO-coated glass substrates (Ossila, 20 Ω) were ultrasonically cleaned successively in acetone, DI water, and isopropanol, and dried in a N_2 stream. The ITO-glass was used as the working electrode in a three-electrode cell (Pt counter, Ag/AgCl reference) containing the deposition solution and cycled using cyclic voltammetry between −0.1 and 0.9 V for a prescribed number of cycles at a scan rate of 50 mV/s, during which the amount of cycling charge increased with each cycle, indicating progressive electrodeposition of PDPA. Areal capacities during cycling are approximately 15−20 mC/cm^2. After electrodeposition, PSSH doped samples were washed with ethanol, DI water, and 2-propanol before being dried in a N_2 stream. MSH and TSH doped samples were not washed with water as they were more susceptible to delamination during water rinsing.

PDPA Characterization

A three-electrode cell consisting of a quartz-windowed cuvette, Pt-wire counter electrode, and Ag/AgCl reference electrode was used to collect transmittance spectra at −0.1 and 0.95 V vs Ag/AgCl in 0.2 M $LiClO_4$ (Alfa-Aesar, anhydrous 99%) dissolved in PC (Alfa-Aesar, anhydrous, 99.5%) (Scheme 1). Transmittance was measured using a Cary 5000 UV−vis−NIR spectrophotometer between 300 and 1700 nm. Baseline 100% transmittance scans were performed with an empty cuvette (only quartz windows in the beam path). In select instances, a single wavelength (700 nm) was measured during potentiostatic cycling, with no cuvette baseline correction (see Figure S4, Supporting Information). Scanning electron microscopy (SEM) images were observed by a Zeiss Supra 55VP instrument with an Oxford 80 mm^2 energy dispersive X-ray spectroscopy (EDX) detector and Aztec software.

Optical images were obtained with an optical microscope (Bruker) and corrected for optical aberrations. FT-IR absorption spectra were measured on thin solid films by using an attenuated total internal reflectance (ATR) geometry (Bruker LUMOS). Resonance Raman spectroscopy was performed on PDPA thin films using a combination of dispersive (home-built confocal microscope or Renishaw InVia) and FT (Bruker RAM II) methods with excitation from ∼350−1064 nm. All samples showed large fluorescence backgrounds that were removed by either fitting polynomial functions and baseline subtraction or the pseudosecond derivative method. Spectra were also corrected by accounting for thin film absorption to compare the relative intensities.

s-SNOM imaging of as-prepared PDPA thin films is performed using an integrated tapping-mode atomic force microscope (AFM, Ω ∼270 kHz, 80 nm dither) and a near-field microscope system (Neaspec GmbH). A tunable, linearly polarized quantum cascade laser (QCL) (MIRcat-QT-Z-2400, Daylight Solutions, Inc.) generates IR radiation with frequencies of ∼1250−1850 cm^{-1}, ca. 0.1 cm^{-1} line width that was introduced to the microscope system and focused using a parabolic mirror (NA = 0.46) at the tip−sample interface (30° excitation grazing incidence angle). IR scattering is detected by using MCT photodiodes (Kolmar Technologies, Inc.) cooled by liquid nitrogen in a pseudoheterodyne interferometric detection geometry. Simultaneous IR excitation amplitude and phase are recorded along with the AFM topographic and phase shift images by raster scanning samples. The detector output is demodulated at higher harmonics (amplitude, S_3 and S_4, and phase, Ω_3 and Ω_4) to exclude far-field contributions.

https://doi.org/10.1021/acsaom.3c00421
ACS Appl. Opt. Mater. 2024, 2, 361−367

■ ASSOCIATED CONTENT

Supporting Information

The Supporting Information is available free of charge at https://pubs.acs.org/doi/10.1021/acsaom.3c00421.

Electrochemical data, optical images, SEM images, UV−vis−NIR transmittance spectra, and calculated parameters, spectroelectrochemical cycling data, XPS depth profiles and spectra, resonance Raman spectra, time-dependent Raman intensity simulations, frequency-dependent s-SNOM images of PDPA (PDF)

■ AUTHOR INFORMATION

Corresponding Authors

Terefe G. Habteyes − *Department of Chemistry, University of New Mexico, Albuquerque, New Mexico 87131, United States;* orcid.org/0000-0001-5978-6464; Email: habteyes@unm.edu

John K. Grey − *Sandia National Laboratories, Albuquerque, New Mexico 87185, United States;* orcid.org/0000-0001-7307-8894; Email: jkgrey@sandia.gov

Nathan T. Hahn − *Sandia National Laboratories, Albuquerque, New Mexico 87185, United States;* orcid.org/0000-0001-6187-4068; Email: nthahn@sandia.gov

Authors

Simranjit Grewal − *Sandia National Laboratories, Albuquerque, New Mexico 87185, United States*

Wassie M. Takele − *Department of Chemistry, University of New Mexico, Albuquerque, New Mexico 87131, United States*

Dongchang Chen − *Department of Chemistry, University of New Mexico, Albuquerque, New Mexico 87131, United States*

Complete contact information is available at: https://pubs.acs.org/10.1021/acsaom.3c00421

Notes

The authors declare no competing financial interest.

■ ACKNOWLEDGMENTS

This work was supported by the Laboratory Directed Research and Development program at Sandia National Laboratories, a multimission laboratory managed and operated by National Technology and Engineering Solutions of Sandia, LLC, a wholly owned subsidiary of Honeywell International, Inc., for the U. S. Department of Energy's National Nuclear Security Administration under Contract DE-NA-0003525. This written work is authored by an employee of NTESS. The employee, not NTESS, owns the right, title, and interest in and to the written work and is responsible for its contents. Any subjective views or opinions that might be expressed in the written work do not necessarily represent the views of the U. S. Government. The publisher acknowledges that the U. S. Government retains a nonexclusive, paid-up, irrevocable, worldwide license to publish or reproduce the published form of this written work or allow others to do so, for U. S. Government purposes. The DOE will provide public access to results of federally sponsored research in accordance with the DOE Public Access Plan. We also acknowledge contributions from Melissa Meyerson for acquisition of XPS spectra and TGH acknowledges support from the National Science Foundation Grant (#2154617) to obtain the Quantum Cascade Laser used for s-SNOM imaging.

■ REFERENCES

(1) Wu, S.; Sun, H.; Duan, M.; Mao, H.; Wu, Y.; Zhao, H.; Lin, B. Applications of Thermochromic and Electrochromic Smart Windows: Materials to Buildings. *Cell Rep. Phys. Sci.* **2023**, *4* (5), No. 101370.

(2) Tällberg, R.; Jelle, B. P.; Loonen, R.; Gao, T.; Hamdy, M. Comparison of the Energy Saving Potential of Adaptive and Controllable Smart Windows: A State-Of-The-Art Review and Simulation Studies of Thermochromic, Photochromic and Electrochromic Technologies. *Solar Energy Mater. Solar Cells* **2019**, *200*, No. 109828.

(3) *Windows*, U. S. Office of Energy Efficiency and Renewable Energy, https://www.energy.gov/eere/buildings/windows (accessed 2023-11-01).

(4) Kim, J.; Remond, M.; Kim, D.; Jang, H.; Kim, E. Electrochromic Conjugated Polymers for Multifunctional Smart Windows with Integrative Functionalities. *Adv. Mater. Technol.* **2020**, *5* (6), No. 1900890.

(5) Khandelwal, H.; Schenning, A. P. H. J.; Debije, M. G. Infrared Regulating Smart Window Based on Organic Materials. *Adv. Energy Mater.* **2017**, *7* (14), No. 1602209.

(6) Li, X.; Perera, K.; He, J.; Gumyusenge, A.; Mei, J. Solution-Processable Electrochromic Materials and Devices: Roadblocks and Strategies Towards Large-Scale Applications. *J. Mater. Chem. C* **2019**, *7* (41), 12761−12789.

(7) Argun, A. A.; Cirpan, A.; Reynolds, J. R. The First Truly All-Polymer Electrochromic Devices. *Adv. Mater.* **2003**, *15* (16), 1338−1341.

(8) Guay, J.; Paynter, R.; Dao, L. H. Synthesis and Characterization of Poly(Diarylamines): A New Class of Electrochromic Conducting Polymers. *Macromolecules* **1990**, *23* (15), 3598−3605.

(9) Chung, C.-Y.; Wen, T.-C.; Gopalan, A. Identification of Electrochromic Sites in Poly(Diphenylamine) using a Novel Absorbance−Potential−Wavelength Profile. *Electrochim. Acta* **2001**, *47* (3), 423−431.

(10) Kim, M. H.; Bae, D. H.; Choi, H. J.; Seo, Y. Synthesis of Semiconducting Poly(Diphenylamine) Particles and Analysis of their Electrorheological Properties. *Polymer* **2017**, *119*, 40−49.

(11) Athawale, A. A.; Deore, B. A.; Chabukswar, V. V. Studies on Poly(Diphenylamine) Synthesized Electrochemically in Nonaqueous Media. *Mater. Chem. Phys.* **1999**, *58* (1), 94−100.

(12) Hayat, U.; Bartlett, P. N.; Dodd, G. H.; Barker, J. Electrochemical Synthesis and Study of Polydiphenylamine. *J. Electroanal. Chem. Interface Electrochem.* **1987**, *220* (2), 287−294.

(13) Jana, T.; Nandi, A. K. Sulfonic Acid Doped Thermoreversible Polyaniline Gels. 2. Influence of Sulfonic Acid Content on Morphological, Thermodynamical, and Conductivity Properties. *Langmuir* **2001**, *17* (19), 5768−5774.

(14) Jayakannan, M.; Annu, S.; Ramalekshmi, S. Structural Effects of Dopants and Polymerization Methodologies on the Solid-State Ordering and Morphology of Polyaniline. *J. Polym. Sci., Part B: Polym. Phys.* **2005**, *43* (11), 1321−1331.

(15) Wen, T.-C.; Chen, J.-B.; Gopalan, A. Soluble and Methane Sulfonic Acid Doped Poly(Diphenylamine) - Synthesis and Characterization. *Mater. Lett.* **2002**, *57* (2), 280−290.

(16) Nagarajan, S.; Santhosh, P.; Sankarasubramanian, M.; Vasudevan, T.; Gopalan, A.; Lee, K.-P. UV-vis Spectroscopy for Following the Kinetics of Homogeneous Polymerization of Diphenylamine in p-Toluene Sulfonic Acid. *Spectrochim. Acta, Part A* **2005**, *62A* (1−3), 420−430.

(17) Athawale, A. A.; Deore, B. A.; Chabukswar, V. V. Studies on Poly(Diphenylamine) Synthesized Electrochemically in Nonaqueous Media. *Mater. Chem. Phys.* **1999**, *58* (1), 94−100.

(18) Zhang, T.; Qi, H.; Liao, Z.; Horev, Y. D.; Panes-Ruiz, L. A.; Petkov, P. S.; Zhang, Z.; Shivhare, R.; Zhang, P.; Liu, K.; Bezugly, V.;

Liu, S.; Zheng, Z.; Mannsfeld, S.; Heine, T.; Cuniberti, G.; Haick, H.; Zschech, E.; Kaiser, U.; Dong, R.; Feng, X. Engineering Crystalline Quasi-Two-Dimensional Polyaniline Thin Film with Enhanced Electrical and Chemiresistive Sensing Performances. *Nat. Commun.* **2019**, *10* (1), 4225.

(19) do Nascimento, G. M.; Pereira da Silva, J. E.; Cordoba de Torresi, S. I.; Temperini, M. L. A. Comparison of Secondary Doping and Thermal Treatment in Poly(diphenylamine) and Polyaniline Monitored by Resonance Raman Spectroscopy. *Macromolecules* **2002**, *35* (1), 121−125.

(20) Eigner, A. A.; Jones, B. H.; Koprucki, B. W.; Massari, A. M. Ground-State Structural Dynamics in Doped and Undoped Polyaniline Films Probed by Two-Dimensional Infrared Vibrational Echo Spectroscopy. *J. Phys. Chem. B* **2011**, *115* (16), 4583−4591.

(21) Santana, H. d.; Matos, J. d. R.; Temperini, M. L. A. Characterization of Polydiphenylamine Electrochemically Synthesized by Spectroscopic and Thermal Techniques. *Polym. J.* **1998**, *30*, 315−321.

(22) Eigner, A. A.; Jones, B. H.; Koprucki, B. W.; Massari, A. M. Static and Dynamic Structural Memory in Polyaniline Thin Films. *J. Phys. Chem. B* **2011**, *115* (27), 8686−8695.

(23) Koch, F. P. V.; Rivnay, J.; Foster, S.; Müller, C.; Downing, J. M.; Buchaca-Domingo, E.; Westacott, P.; Yu, L.; Yuan, M.; Baklar, M.; Fei, Z.; Luscombe, C.; McLachlan, M. A.; Heeney, M.; Rumbles, G.; Silva, C.; Salleo, A.; Nelson, J.; Smith, P.; Stingelin, N. The Impact of Molecular Weight on Microstructure and Charge Transport in Semicrystalline Polymer Semiconductors−Poly(3-Hexylthiophene), a Model Study. *Prog. Polym. Sci.* **2013**, *38* (12), 1978−1989.

(24) Andrew, T. L.; Swager, T. M. Reduced Photobleaching of Conjugated Polymer Films through Small Molecule Additives. *Macromolecules* **2008**, *41* (22), 8306−8308.

(25) Jensen, J.; Madsen, M. V.; Krebs, F. C. Photochemical Stability of Electrochromic Polymers and Devices. *J. Mater. Chem. C* **2013**, *1* (32), 4826−4835.

(26) Chandrasekhar, P.; Zay, B. J.; Lawrence, D.; Caldwell, E.; Sheth, R.; Stephan, R.; Cornwell, J. Variable-Emittance Infrared Electrochromic Skins Combining Unique Conducting Polymers, Ionic Liquid Electrolytes, Microporous Polymer Membranes, and Semiconductor/Polymer Coatings, for Spacecraft Thermal Control. *J. Appl. Polym. Sci.* **2014**, *131* (19), 40850.

https://doi.org/10.1021/acsaom.3c00421
ACS Appl. Opt. Mater. 2024, 2, 361−367